AGU ADVANCING EARTH AND SPACE SCIENCES

Water Resources Research

RESEARCH ARTICLE
10.1029/2022WR033970

Evidence and Controls of the Acceleration of the Hydrological Cycle Over Land

Y. Wang[1], **N. Meili**[1,2], **and S. Fatichi**[1]

[1]Department of Civil and Environmental Engineering, National University of Singapore, Singapore City, Singapore, [2]Future Cities Laboratory Global, Singapore-ETH Centre, Singapore City, Singapore

Key Points:

- Several methods to approximate soil water residence time from commonly available hydrological variables are introduced and compared
- The global terrestrial water cycle is currently accelerating and projected to do so in future climate scenarios
- Precipitation changes play a more dominant role in the acceleration of the terrestrial water cycle when compared to evapotranspiration

Supporting Information:

Supporting Information may be found in the online version of this article.

Correspondence to:

Y. Wang,
yiranw@u.nus.edu

Citation:

Wang, Y., Meili, N., & Fatichi, S. (2023). Evidence and controls of the acceleration of the hydrological cycle over land. *Water Resources Research*, *59*, e2022WR033970. https://doi.org/10.1029/2022WR033970

Received 26 OCT 2022
Accepted 30 JUL 2023

Author Contributions:

Conceptualization: Y. Wang, N. Meili, S. Fatichi
Data curation: Y. Wang
Formal analysis: Y. Wang
Investigation: Y. Wang, N. Meili, S. Fatichi
Methodology: Y. Wang, N. Meili, S. Fatichi
Resources: Y. Wang
Software: Y. Wang, S. Fatichi
Writing – original draft: Y. Wang
Writing – review & editing: Y. Wang, N. Meili, S. Fatichi

Abstract Investigating modifications in the hydrological cycle is essential to understand the impacts of climate change on ecosystems. This study assesses the change in the velocity of the water cycle over land at the global scale, whereas previous studies have mostly focused on changes in the atmospheric water cycle. The hydrological acceleration is quantified by a decrease in average residence time (RT) of water in the first meter of soil. The soil water RT is shown to be sensitive to the soil texture and seasonality of hydroclimatic variables. Despite substantial local variability, most of the RTs are in the range of 50–300 days. The global mean soil water RT declined at a rate of −2.30 and −0.36 days decade^{-1} (−1.6 to 1.0 days decade^{-1} the range of nine models) from 2001 to 2020 as measured by reanalysis and CMIP6 simulations for the historical scenario, respectively, which corresponds to −6.8 and −1.1 days °C^{-1} when expressed per degree of global warming over land. This acceleration is projected to continue at a rate of −1.35 days decade^{-1} (−3.4 to 0.0 days decade^{-1} the range of nine models) or −2.2 days °C^{-1} during the period 2015–2100 under the most extreme emission scenario: SSP 585. Changes in precipitation dominantly drive the acceleration of the terrestrial water cycle compared to changes in evapotranspiration. Rising temperatures and increasing carbon dioxide have opposite effects on the speed of the terrestrial water cycle with compensatory roles keeping RT relatively unchanged in the absence of PR trends.

1. Introduction

The velocity of the hydrological cycle is important for studying impacts of climate change on water resources and ecosystem functions because it affects the exchange of water between the atmosphere and the land and the RT of water in the atmosphere and in the soil where it can impact biogeochemical transformations and solute transport (e.g., Bickel & Or, 2020; Humphrey et al., 2021; Ohmura & Wild, 2002; Sprenger et al., 2019). Furthermore, changes in the hydrological cycle are closely related to changes in vegetation productivity and preservation of water resources. A significant positive correlation exists between evapotranspiration (ET), the main water flux in the global land hydrological cycle, and gross primary production (GPP), as leaf stomata are the essential link for the exchange of carbon dioxide and water vapor between land and air (Brümmer et al., 2012; Gerten et al., 2004; Katul et al., 2012; Oki & Kanae, 2006; K. Wang & Dickinson, 2012). The IPCC report indicates that continued global warming is expected to affect the global water cycle and that precipitation (PR) and surface runoff in most terrestrial regions become increasingly seasonally variable, which can affect the soil water residence time (IPCC, 6AR, 2021; Figure TS.12, Arias et al., 2021). Many previous studies have focused on the acceleration of the water cycle in the atmosphere reporting shorter RT of water vapor in the atmosphere (Allan et al., 2014; Held & Soden, 2006; Ohmura & Wild, 2002; Sherwood & Fu, 2014). However, changes in the velocity of the water cycle over land have been less studied because of the complexity associated with the multiple terrestrial hydrological fluxes and characterization of RT in the soil (Huntington, 2006; Huntington et al., 2018). Changes in precipitation, and its partition between evapotranspiration and runoff at the land surface are indeed expected to alter soil moisture and RTs (Wu et al., 2013; D. Yang et al., 2021).

The use of water for agriculture as an anthropogenic intervention can further complicate the analysis of the terrestrial water cycle, as irrigation can modify groundwater recharge or return water vapor to the atmosphere through crop transpiration, thus altering the natural water exchange between land and air (Haddeland et al., 2006; Ozdogan et al., 2010; Pokhrel et al., 2012; Puma & Cook, 2010; Tang et al., 2007). Consequently, studying changes in the velocity of the terrestrial water cycle is still an open problem, as the velocity of the water cycle over land is subject to great regional variability and higher uncertainty than in the atmosphere.

Soil moisture (SM) is an important element of the terrestrial water cycle and it is a critical factor for studies focusing on vegetation dynamics, agricultural production, and climatology (Cavagnaro, 2016; Humphrey et al., 2021; Robinson et al., 2008; Vereecken et al., 2008). The water content in the soil is closely related to water stress in plants, thus affecting plant photosynthesis and respiration, with implications for vegetation productivity and the global carbon cycle (Anav et al., 2015; Byrne & O'Gorman, 2015; Greve et al., 2014; Greve & Seneviratne, 2015). In addition, SM acts as a solvent for fertilizers and contaminants and has significant impacts on crop growth and yield (Kaur et al., 2018; Yan et al., 2020). Furthermore, it has been shown that global droughts have been exacerbated by the adverse effects of reduced SM on temperature, precipitation, and relative humidity (Bateni & Entekhabi, 2012; Berg et al., 2016; Hirschi et al., 2014; Seneviratne et al., 2006; Sheffield & Wood, 2008; Yin et al., 2014). Here, average soil water RT is chosen as the main metric to evaluate the speed of the terrestrial water cycle, where a reduction in RT represents an acceleration of the terrestrial hydrological cycle.

Previous studies quantifying the effects of climate change on the velocity of the terrestrial water cycle have mostly used PR and ET to assess if an acceleration occurred (Huntington et al., 2018; Roderick et al., 2014), with less consideration of surface runoff and soil leakage (LK). In this study, we combine values of SM, ET, surface runoff and LK to refine the calculation of soil water RT based on water fluxes available from different data and modeling products. We used historical reanalysis data, CMIP6 model outputs, and mechanistic ecohydrological modeling to achieve the following research aims: (a) test the sensitivity of soil water RT to meteorological forcing and soil texture; (b) identify the spatial and temporal changes in soil water RT under historical conditions and future scenarios; (c) investigate the main reasons for a velocity change of the terrestrial water cycle by exploring the response of soil water RT to increased temperature, increased CO_2, PR changes, and the associated variations in ET and GPP under future climate conditions.

2. Methods and Data

As there are many uncertainties involved in the analysis of changes in the velocity of the terrestrial water cycle here, we combine a range of methodological approaches to address the challenge from multiple perspectives. Specifically, after having specified the non-trivial (and approximated) computation of soil water RT (Section 2.1), we use data-driven observations from reanalysis to look at past changes (Section 2.2) and CMIP6 model simulations (Section 2.3) to look at projected future changes. However, using solely a global perspective falls short of identifying the mechanisms driving the RT modifications as all variables concurrently change in the CMIP6 simulations. This does not allow an unambiguous partitioning of the causes of RT changes. Therefore, we also run dedicated numerical experiments at the local scale with a terrestrial biosphere model (Section 2.4) to quantify the role of meteorological variables in driving RT changes from a process-based standpoint.

2.1. Computation of Residence Time of Soil Water

This article examines past and future changes in soil water RT to quantify changes in the velocity of the water cycle over land. The RT of soil water is derived directly from the components of the terrestrial water balance, which can be written in its essential form for a one-dimensional soil column as (Brutsaert, 2005; Huntington et al., 2018):

$$\frac{dS}{dt} = PR - ET - Q \tag{1}$$

Where dS/dt represents the change in soil water storage over a certain time period, PR is the precipitation, ET is the evapotranspiration, and Q is the discharge which can include surface and subsurface components. We can further subdivide Q and ET into their essential subcomponents as:

$$Q = R_{sur} + LK \tag{2}$$

$$ET = EG + E_{in} + T \tag{3}$$

Where R_{sur} is the surface runoff, LK is the soil leakage at the bottom of the soil column, EG represents the evaporation from ground, E_{in} is the evaporation from intercepted water on the plant canopy, and T is the transpiration from vegetation.

In a steady and mass conservative system, the average RT is defined as the volume divided by the flux (e.g., Dingman, 2015). Assuming a reference period of a week or a month or a year, the true unknown RT is approximated with the average SM for a given soil depth over this period (which partially discounts for the lack of stationarity) and the average of all the inputs or outputs (e.g., the water flux) from the soil column. The term PR—E_{in}—Rsurh, can be considered as the water input to the soil (Equation 4), that is, PR minus evaporation from interception and surface runoff that does not enter in the soil, as Rsurh is defined as the infiltration excess runoff (Hortonian runoff). From the soil column perspective, EG, T, and LK can be classified as outputs (Equation 5). Note, the case of ignoring LK is also considered and discussed in Section 3.1 (Equation 6). The RT can be approximated by dividing the average volume of water in the soil S by either the input to or output from the soil column as:

$$RT_{in} = \frac{S}{PR - E_{in} - R_{surh}} \tag{4}$$

$$RT_{out} = \frac{S}{EG + T + LK} \tag{5}$$

$$RT_{out-LK} = \frac{S}{EG + T} \tag{6}$$

The units of S and RT are [mm] and [day], respectively. As the soil system is rarely in a steady state over time periods of 1 week to 1 year (e.g., S changes throughout this period), both Equations 4 and 5 are only approximations of the true RT and they might slightly differ in their estimate of RT, even though in a system in dynamic equilibrium they should provide consistent results. Note that Equation 5 is theoretically a more robust approximation as EG + T + LK is never exactly zero, which is different from the denominator of Equation 4 that is exactly zero when PR = 0 over a certain period of time. Additionally, the soil water content S is computed by specifying a given depth, which adds another level of uncertainty. However, even though RT is forcefully approximated in this study, its approximation is an advancement with regards to previous literature which utilizes the difference between PR and ET to estimate changes in water availability (Greve & Seneviratne, 2015) or the sum of PR and ET to compute the water cycle intensity and its acceleration (Huntington et al., 2018). In this article, we use these two (Equations 4 and 5) more refined, although still approximated, methods to compute RT at monthly or annual scale and we also use some simplified formulations where RT is computed based on the knowledge of PR or total ET as the only available flux (Equations 7 and 8).

$$RT_{ET} = \frac{S}{ET} \tag{7}$$

$$RT_{PR} = \frac{S}{PR} \tag{8}$$

Based on this multiplicity of definitions, a comparison among different methods for computing water cycle intensity and RTs has been carried out to investigate the sensitivity of RTs to the exact calculation method and thus its relative robustness. This aspect is further discussed in Section 3.1. Note that the calculation of RT in ERA5 and CMIP6 data sets is based on the annual average of the hydrological variables, which is done to prevent unrealistically high values of monthly RT due to zero or nearly zero precipitation in a given month. A problem that does not occur whenever Equation 5 can be used.

2.2. Data From Reanalysis

We obtained global hydroclimatic data (names of variables provided in Table S1 in Supporting Information S1) at a monthly frequency from the ERA5-Land reanalysis product to analyze spatial and temporal variations in ET, PR, SM, and RT of soil water for the period 2001–2020 (available at https://www.ecmwf.int/en/era5-land). Reanalysis combines model results and observations collected on a global scale to form an accurate and comprehensive data set that reflects climate conditions under historical scenarios (Hersbach et al., 2020). ERA5-Land is an updated version of the ERA5 reanalysis product with a grid resolution of 9 km, focusing on the water and energy cycles on the land surface (Muñoz-Sabater et al., 2021). The reason for limiting the analysis to 2001–2020 is that when exploring changes in SM over the extended time period from 1980 to 2020, we detected a sharp

drop in SM around 2000, which corresponds to an artifact of how the SM in the reanalysis product is computed which is still under investigation (correspondence with the product developers). It is indeed unrealistic to expect a marked change in SM over the duration of a year and it is presumably due to different assimilated products used by ERA5-Land to estimate SM from 2000 onwards. To reduce the impact of methodological changes on the accuracy of the results, we limited the analysis to the period 2001–2020. Furthermore, we only analyzed areas with latitudes between 65°N and 65°S to minimize the impacts of frozen ground and seasonal snow cover. Additionally, we masked out areas with less than 100 mm annual PR because as PR approaches zero and is rapidly removed by ET, SM tends to be low and constant, leading to inaccurate estimates of RT using monthly and sometimes annual values (e.g., the computed RT with Equation 4 will be infinite for null PR). As extreme values can have a significant impact on the calculation of the global mean, we also computed the global average by removing extreme values and selecting three different percentage thresholds (0.1%–99.9%, 1%–99% and 5%–95%). We found that the selection of different threshold ranges had only a minimal impact on the calculation of the average RT trends. Therefore, in subsequent global mean calculations, we chose the 1%–99% interval of the RT distribution to compute trends and statistics. The percentages of land area showing accelerating/deaccelerating trends in ET, PR, SM and RT is calculated based only on the analyzed regions, that is, 65°N to 65°S excluding arid areas and the RT values beyond the 1%–99% percentiles (specific locations of outliers are plotted in Figure S1 in Supporting Information S1). The excluded areas represent 27% of the total global land area. As LK is not among the fluxes directly provided by ERA5, the RT of soil water for this product was calculated according to Equation 4. A soil depth of 1 m was chosen as it is representative of the soil layer that interacts in a relatively fast and frequent way with the atmosphere and where most plant roots are located, thus affecting natural vegetation and agricultural productivity (Fan et al., 2017; Jackson et al., 1996).

2.3. CMIP6 Simulations

To further evaluate the current and future changes in soil water RT, we acquired monthly simulation outputs from the Sixth Coupled Model Intercomparison Project (CMIP6) under the historical scenario and the high Shared Socioeconomic Pathway SSP 585 (available at https://esgf-node.llnl.gov/search/cmip6/). CMIP6 provides an integrated overview of the climate variables (names of variables provided in Table S1 in Supporting Information S1) produced by various climate models under different simulated conditions, with SSP 585 implying the high end of the range of future emission pathways (Almazroui et al., 2021; Eyring et al., 2016; Popp et al., 2017). Nine General Circulation Models (GCMs) included in CMIP6 were selected based on the availability of the variables to calculate soil water RTs in the period 2001–2020 and 2015–2100. The simulations provided by CMIP6 for the historical scenario ended in 2014, and we used the data from the SSP 585 scenario for the 2015–2020 period to better align the comparison of the historical CMIP6 conditions with the reanalysis study period. Differences among emission scenarios in the first five years (2015–2020) are practically indistinguishable (IPCC, 6AR, 2021, Fig. 1.28, Chen et al., 2021) and they do not affect the changes in the simulated hydrological variables. The RT was computed according to Equation 5, as all variables were available for its estimation in the CMIP6 models (Table S1 in Supporting Information S1), which is different for the case of the reanalysis data (Equation 4). The RT change rate was assessed over time (days decade^{-1}) and as a function of global temperature change (days °C^{-1}). The relationship between RT change and global temperature change was calculated by dividing the linear slope of the change in RT over time (days decade^{-1}) by the linear slope of the change in global mean annual land temperature over time (°C decade^{-1}).

Furthermore, we calculated the mass budget closure for each model (Figure S2 in Supporting Information S1) to ensure robustness in the calculation of RT. The degree of model closure is assessed through the percentage of PR-ET-Q to PR (Figure S2 in Supporting Information S1). The mass budget closure of five CMIP6 models is zero except over coastal regions where the grid cell might have a fraction covered by sea and ET might be partially contributed by seawater, but for four models the mass budget is not fully closed also in certain inland areas, with discrepancies of up to 7%–8%. Here we retain all nine models, but also provide an analysis and discussion of the results excluding models where the mass budget is not exactly closed in Section 3.3. The nine GCMs and the scenario details are listed in Table 1.

2.4. T&C Model

In addition to the large-scale analysis, the ecohydrological model Tethys-Chloris (T&C) is used for an in-depth assessment of the processes controlling soil water RT as for instance the influence of soil texture and climate

Table 1
List of CMIP6 General Circulation Models (GCMs) Selected for the Analysis

Model	Resolution	Run	Period	Soil depth [m]
CanESM5	500 km	r1i1p1f1	January 2001–December 2100	0.35
MIROC6	250 km	r1i1p1f1	January 2001–December 2100	0.63
CMCC-CM2-SR5*	100 km	r1i1p1f1	January 2001–December 2100	1.04
CMCC-ESM2*	100 km	r1i1p1f1	January 2001–December 2100	1.04
CESM2-WACCM	100 km	r2i1p1f1	January 2001–December 2100	1.06
CNRM-ESM2-1	250 km	r1i1p1f2	January 2001–December 2100	0.90
GFDL-ESM4*	100 km	r1i1p1f1	January 2001–December 2100	0.90
BCC-CSM2-MR*	100 km	r1i1p1f1	January 2001–December 2100	1.04
TaiESM1	100 km	r1i1p1f1	January 2001–December 2100	1.04

Note. The soil layers closest to 1 m depth were selected for each model and the water content was rescaled to exactly 1 m in this study to allow comparison of results in terms of RT. The models with an asterisk do not perfectly close the mass budget.

variables. T&C is a mechanistic ecohydrological model that jointly simulates the hydrological and carbon cycles for various climates and ecosystems (Fatichi et al., 2012a, Fatichi et al., 2012b, 2021). Its ability to simulate carbon and water fluxes and the exchange of energy at the land-surface has been validated in multiple previous studies using eddy covariance flux tower observations and other hydrological and ecohydrological data sets from sites with different vegetation and climate (e.g., Botter et al., 2021; Fatichi et al., 2012b, 2014, 2016; Manoli et al., 2018; Pappas et al., 2016; Paschalis et al., 2017, 2018, 2022). The T&C model can mechanistically simulate the response of important ecohydrological variables such as ET and GPP to changes in atmospheric forcing. By varying one or two specific climate variables in targeted T&C simulations, their influence on the hydrological cycle and ecosystem response can be isolated and quantified. Hence, T&C is used in this research for three purposes: (a) to evaluate the influence of different methodologies in computing RT, as it can provide all the necessary variables to evaluate differences among the definitions of RT (Section 3.1); (b) to evaluate the influence of soil textural conditions and soil depth as well as seasonality of meteorological variables in the computation of soil water RT (Section 3.1), and (c) to analyze the effect of changes in temperature, CO_2, and PR conditions on soil water RT (Section 3.4). Equation 5 is used as the most accurate benchmark for the estimation of soil water RT in Sections 3.1 and 3.4.

Numerical experiments were conducted with T&C to test the response of RT to changes in soil texture and climatic conditions. First, we run a sensitivity analysis of soil water RT, computed at the monthly scale, to soil texture to illustrate its variability for a fixed climate forcing and vegetation. We used for this purpose hourly meteorological time series for Zurich from 1981 to 2012 and a representative C_3 grassland cover. We selected five different soil texture classes: clay, clay-loam, sand, sandy loam, and silt, which cover a wide range of soil conditions (Saxton & Rawls, 2006). Three different soil depths (0.1 m/1 m/2 m) were used for analyzing the seasonal patterns of RT variations.

Using meteorological observations, soil and vegetation boundary conditions from 118 sites worldwide spanning multiple biomes and climatic regions (e.g., Fatichi & Pappas, 2017; Mastrotheodoros et al., 2017; the locations of the 118 sites are plotted in Figure S3 in Supporting Information S1 and detailed site information is provided in Table S2 in Supporting Information S1), four different soil depths (0.1 m/0.3 m/0.5 m/1 m) were used to further explore the sensitivity of computed RT to the selection of soil depth. In addition, for the same sites RT_{in}, RT_{out}, RT_{ET}, and RT_{PR} were computed to assess the influence of the calculation method on the monthly scale RT.

Second, we assessed the sensitivity of RT to changing climatic conditions. For this purpose, we simulated the impacts of changing temperature, PR, and atmospheric CO_2 concentration individually and in combination using the historical climate forcing as a baseline. Specifically, we simulated 8 scenarios for each of the 118 sites, which include increasing the temperature by 1.5° to 4.5°C, increasing CO_2 by 150–250 ppm, and changing PR with a 15% reduction and a 15% increase. These climatic scenarios correspond to the range of changes in climate variables as derived from typical emission scenarios in climate change projections (e.g., Song et al., 2019). The simulations performed with the historical observations were considered as a control scenario, and the simulations

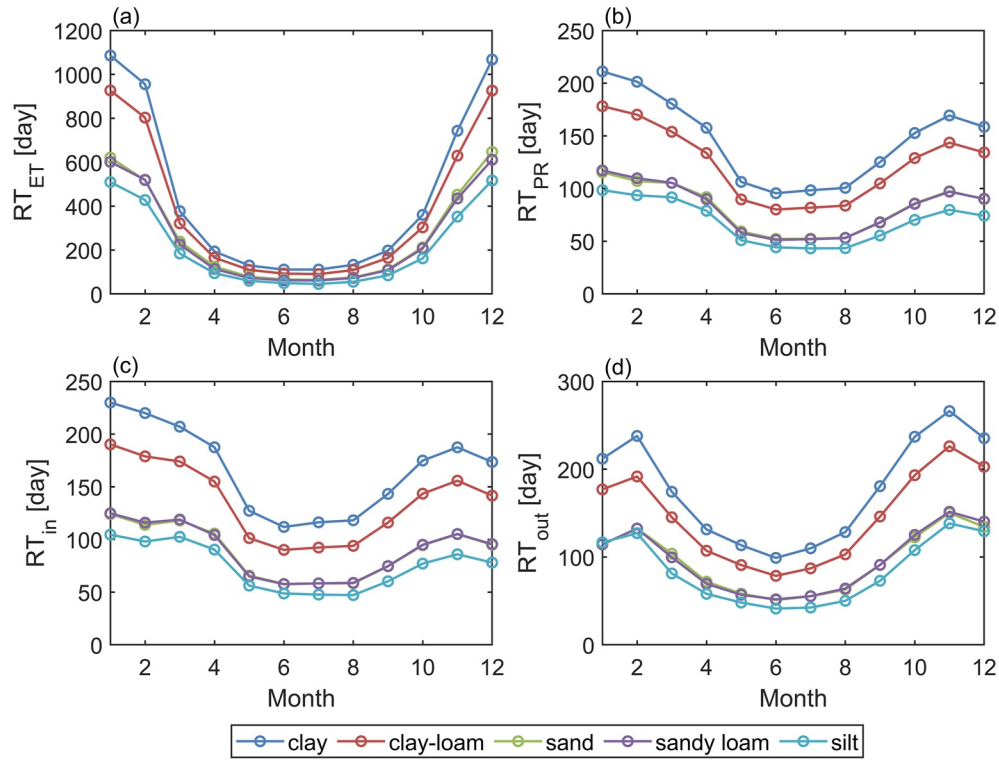

Figure 1. Seasonal changes in soil water RT for different soil textures (clay, clay-loam, sand, sandy loam, and silt). The RTs were calculated with various methods by dividing soil water content at 1 m soil depth by (a) Equation 7, (b) Equation 8, (c) Equation 4, and (d) Equation 5. Simulations were performed for the climate in Zurich over the period from 1981 to 2012 with the T&C model.

conducted under different temperature, PR and CO_2 concentrations were named as perturbed scenarios. We compared the control to the perturbed scenarios to analyze the changes in soil water RT caused by the changes of the different climatic variables.

3. Results

3.1. RT Sensitivity to Soil Texture, Seasonality, and Soil Depth

To explore the sensitivity of soil water RT to changes in meteorological conditions and soil texture, we report the seasonal changes in soil water RT simulated for the location of Zurich with five soil texture types, four soil depths, and considering different formulations to compute the RT. While the soil water RTs computed with the various methodologies differ slightly in their absolute values, they show similar seasonal patterns (Figure S4 in Supporting Information S1). Even using results from the 118 globally distributed sites, different formulations of RT are highly correlated except when the water cycle intensity (i.e., PR + ET) is used (Figure S5 in Supporting Information S1), which suggests that the exact formulation of RT is not critical for analyzing its spatio-temporal variability, and that water cycle intensity might be a too simplistic metric to describe the velocity of the hydrological cycle. As expected, soil type directly influences the magnitude of soil water RT by modifying the soil hydraulic properties and the water redistribution. Using the RT calculated according to Equation 5 from simulations in the location of Zurich as an example (Figure 1d), the RT was longest in clay soils, ranging from 99 to 266 days, followed by clay-loam, sand, and sandy loam soils, with the fastest water turn over in silty soils, ranging from 41 to 138 days. The difference of soil water RT between sand and sandy loam was minimal. Generally differences in RT can be explained by differences in mean soil water content across soil types and in the different effect of viscous forces which modify the soil water retention and hydraulic conductivity functions and thus the redistribution of water in the profile (Assouline & Or, 2013). The high seasonal variablity of soil water RT for the case of Zurich is linked to the local climate characteristics. The RT in the top meter of soil was shortest in

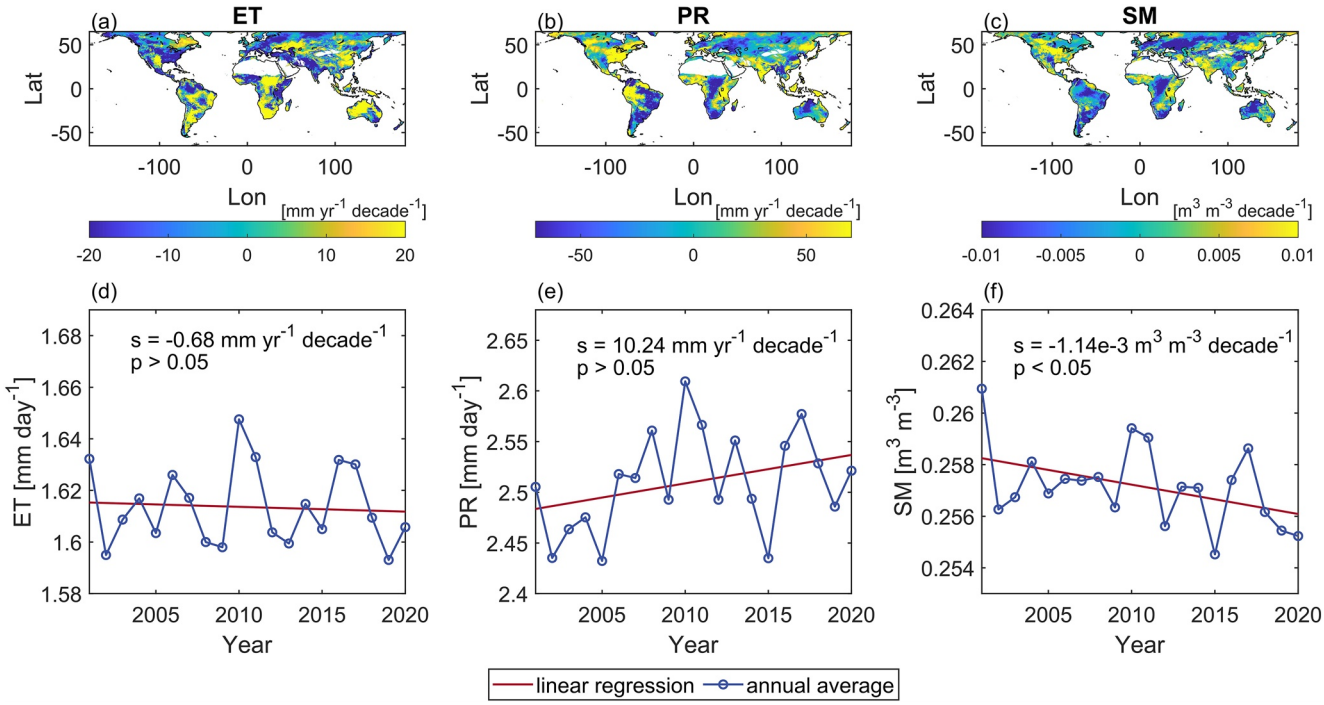

Figure 2. The spatial pattern and temporal trend of land ET, PR, and SM changes derived from ERA5-Land. The maps depict the spatial distribution (65°N–65°S land area excluding arid regions) of change rate of ET (a), PR (b) and SM (c) from 2001 to 2020. The plots (d), (e), and (f) show the temporal trend of land ET, PR and SM from 2001 to 2020 as global annual average. The blue line displays the annual time series of spatial averages, and the red line presents the fitted linear regression. The term s represents the slope of the linear regression and *p* shows its level of significance.

summer (June–August) with an average value of 72 days for the five soil types, and longest in the cold seasons (November–February) with a mean of 166 days (Figure 1d). This is because winter periods are characterized by higher soil water contents and reduced ET rates, while summer in contrary sees much higher transpiration and evaporation rates and lower SMs which reduces the overall RT.

RT calculated with inflow and outflow shows a similar seasonal cycle and the differences in magnitude of RT are minimal. RT calculated simply with the sum of ground evaporation and transpiration is provided for completeness in Figure S6 in Supporting Information S1. As also expected, the magnitude of the RT varies considerably when using different soil depths for its computation. As the soil depth increases, the soil water RT increases as well (Figure S4 in Supporting Information S1). The RT calculated with Equation 5 varies between 4 and 26 days using 0.1 m soil depth (Figure S4d in Supporting Information S1), while it shows values between 85 and 532 days with 2 m soil depth (Figure S4n in Supporting Information S1). However, soil depth has little effect on the seasonal dynamics of soil water RT and average RTs computed at different depths in the 118 locations are highly correlated ($R^2 > 0.98$) (Figure S7 in Supporting Information S1). Hence, a soil depth of 1 m is used for the subsequent analyses.

3.2. Historical Changes in Soil Water RT as Observed by Reanalysis

Using ERA5 -Land over the period 2001–2020, the area of increasing/decreasing ET covers 45.5%/54.5% of the 65°N–65°S target land area, with a significant increasing trend ($p < 0.05$) in 7.9% of the analyzed land area and a significant decreasing trend ($p < 0.05$) in 9.9% of the target land area. Most regions in the Southern Hemisphere showed an increasing trend in ET, while the opposite is true in the Northern Hemisphere (Figure 2a). PR increased/decreased over 53.3%/46.7% of the 65°N–65°S target land area, with a significant increasing trend ($p < 0.05$) over 8.5% of the studied land area and a significant decreasing trend ($p < 0.05$) over 5.9% of the studied land area. There is a clear trend toward increasing PR in the equatorial regions and a decreasing trend in Russia (Figure 2b). The regions with an increasing/decreasing trend in SM represents 45.9%/54.1% of the total land area of 65°N–65°S, with a significant increasing trend ($p < 0.05$) representing 7.0% of the studied land area and a

significant decreasing trend ($p < 0.05$) representing 11.9% of the studied area. Central North America and parts of the Middle East and India showed a clear trend toward an increase SM, while SM decreased in parts of Eastern Europe, North Asia, Central Africa, western Australia, and parts of South America (Figure 2c).

Averaged globally, PR (Figure 2e) over land has an increasing trend over the last two decades, while ET (Figure 2d) and SM (Figure 2f) have decreasing trends albeit at modest rates. Compared to ET with a rate of decrease at -0.68 mm yr^{-1} decade^{-1}, PR increased at a higher rate of 10.24 mm yr^{-1} decade^{-1}. Both changes are not statistically significant though with a p-value larger than 0.05 (the p-value for ET is 0.85, for PR it is 0.13). The lack of a significant ET trend in the ERA5-land contrasts with other recent studies which found positive ET trends (e.g., Liu et al., 2021; Pan et al., 2020). This discrepancy could be the result of the selected period that leads to a smaller trend in ET. Other studies also indicate an overall decreasing trend in global land ET from 1998 to 2008 due to SM constraints in Africa and Australia (Jung et al., 2010), which partially overlap with our chosen study period (2001–2020), and agree with the fact that the overall magnitude of the trend in ET is determined by the period chosen. As a matter of fact, global ET tends to peak in the years following strong El Nino events (1998, 2010, 2015) (Pan et al., 2020). The largest ET with an annual mean of 1.65 mm day^{-1} in our analysis occurred in 2010, the lowest ET of 1.59 mm day^{-1} occurred in 2019. The maximum annual average PR value of 2.62 mm day^{-1} also occurred in 2010, while the minimum value was in 2005 at 2.44 mm day^{-1}. The decreasing SM trend is statistically significant ($p = 0.01 < 0.05$) but the average decrease is only 0.002 m^3 m^{-3} over two decades (Figure 2f).

Based on the above variables, we computed soil water RT from 2001 to 2020 with Equation 4. The annual mean and slope of the twenty-year change in RT is used to represent the overall global change. At a global scale, the computed annual mean RT was 136 days in the period 2001 to 2020. Frequency histograms of RTs in the different latitudes are shown in Figure S8 in Supporting Information S1. The spatial distribution of RTs is closely related to PR. Areas receiving abundant rainfall, such as eastern North America (with RT as short as a few days), Southeast Asia, the Amazon basin, western Europe, have shorter RTs, while RTs were longer for arid areas, such as Central East Australia (with RT at 786 days), western North America, and the Middle East (Figure 3a). Seasonally, both the northern and southern hemisphere have the shortest soil water RT during their respective summer months (Figure S9 in Supporting Information S1). This is due to elevated temperatures and increased solar radiation leading to an increase in ET and thus a reduction in RT in summer. This seasonal pattern can be also found spatially as there is a significant negative correlation between air temperature and RT (R^2 of 0.48 in the 118 sites simulated with T&C, R^2 of 0.32 with the reanalysis datasets, Figure S10 in Supporting Information S1).

While the spatial pattern of average RT is expected, we observed a substantial spatial heterogeneity in the change in RT (Figure 3b). In the analyzed regions, 55.8% of the land area showed an accelerating trend, with 9.5% having a significant accelerating trend (negative slope of soil water RT), while 44.2% of the land area showed a decelerating trend, with 3.5% of regions showing a significant slowdown (positive slope of soil water RT). The trend toward an acceleration of the terrestrial water cycle dominates throughout the northern hemisphere and southern tropics (65°N–23°S), with more than half of the selected region showing a decrease in RT. The highest percentage of regions with accelerating trends (62.3%) was found in the northern hemisphere equatorial region (23°N–0°) where 12.2% of the area showed a significant accelerating trend, followed by the northern hemisphere mid and high latitudes (65°–23°N) with 58.7% and the southern hemisphere equatorial region (23°–65°S) with 56.5%. It is noteworthy that in the mid to high latitudes of the Southern Hemisphere (23°–65°S), more than half of the region shows a trend toward deceleration. There, 71.4%/28.6% of the selected area showed a decelerating/accelerating trend in the terrestrial water cycle, with 6.2% showing a significant decelerating trend. The detailed information about the percentages of regions with RT trends in different latitudinal zones during the historical periods are reported in Table 2. The spatial distribution of regions with significant RT changes were plotted in the Figure S11 in Supporting Information S1. Regions such as western Australia, eastern Europe, western North America, parts of South Africa and southern South America showed a trend toward a deceleration of the hydrological cycle. In contrast, eastern Australia, India, and eastern North America and Central Africa showed an accelerating trend (Figure 3b). As low PR in arid areas and the presence of permafrost in polar regions can lead to RTs tending toward infinity or zero, which may skew the RT distribution when calculating the global mean, three different percentile ranges are used to exclude distribution tails when calculating the annual mean RT. The results show that the three different ranges have little effect on the average calculation of RT change (Figure 3c). Despite substantial geographical differences, the global mean RT (excluding the outliers beyond 1%–99%) has a

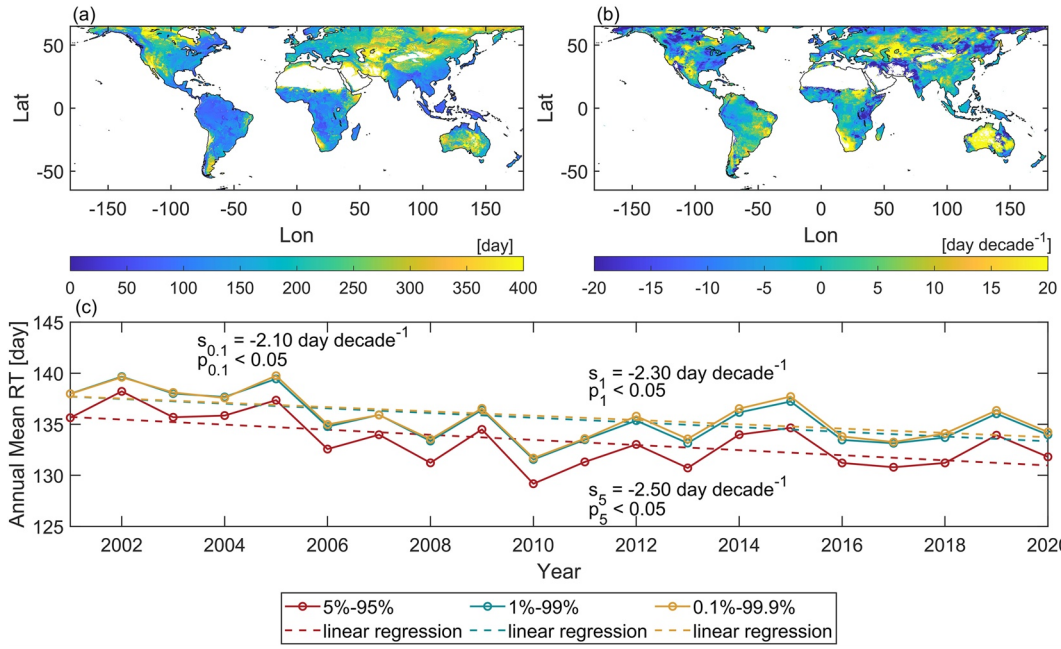

Figure 3. Spatial pattern and temporal trend of soil water RT from 2001 to 2020. The subplot (a) depicts the spatial distribution of annual mean RT by averaging the annual mean RT values over 20 years. The subplot (b) displays the spatial pattern of the change in RT from 2001 to 2020. The area where the PR is less than 100 mm/yr is excluded from the analysis to avoid artifacts in the calculation of RT. Values exceeding 1%–99% of the variable distribution are masked out in the maps. Three colored solid lines in subplot (c) show the actual trends in annual mean RTs excluding distribution tails using three different thresholds, with the dashed line of the same color to represent the fitted linear regression. The term s represents the slope of linear regression and *p* is the significance level. The subscripts of 0.1,1 and 5 represent the statistical results excluding distribution tails outside of 0.1%–99.9%, 1%–99% and 5%–95% percentiles, respectively.

Table 2
Percentage of Regions With Terrestrial Water Cycle Accelerating and Decelerating Trends at Global Scale and in Different Latitudinal Zones in the Historical Period (Reanalysis) and Historical and Future Scenarios (Simulations From CMIP6)

Model	Latitudinal zone	Areas with significant accelerating trends [%]	Areas with accelerating trends [%]	Areas with decelerating trends [%]	Areas with significant decelerating trends [%]
Reanalysis	65°N–65°S	9.5	55.8	44.2	3.5
	65°–23°N	7.8	58.7	41.3	2.3
	23°N–0°	12.2	62.3	37.7	6.3
	0°–23°S	15.4	56.5	43.5	2.8
	23°–65°S	1.1	28.6	71.4	6.2
Multi-GCMs Mean historical scenario	65°N–65°S	5.7	47.0	53.0	9.7
	65°–23°N	4.4	54.7	45.3	3.5
	23°N–0°	6.4	43.6	56.4	18.7
	0°–23°S	6.9	34.9	65.1	16.0
	23°–65°S	9.4	41.8	58.2	11.0
Multi-GCMs Mean SSP 585	65°N–65°S	45.3	64.3	35.7	19.3
	65°–23°N	63.5	80.2	19.8	9.2
	23°N–0°	36.7	56.3	43.7	27.4
	0°–23°S	23.1	45.1	54.9	30.8
	23°–65°S	20.0	43.0	57.0	28.4

Note. The percentage excludes tails of the distribution with RTs exceeding 1%–99%, high/low latitude regions (>|65°|), and arid areas (PR < 100 mm year^{-1}).

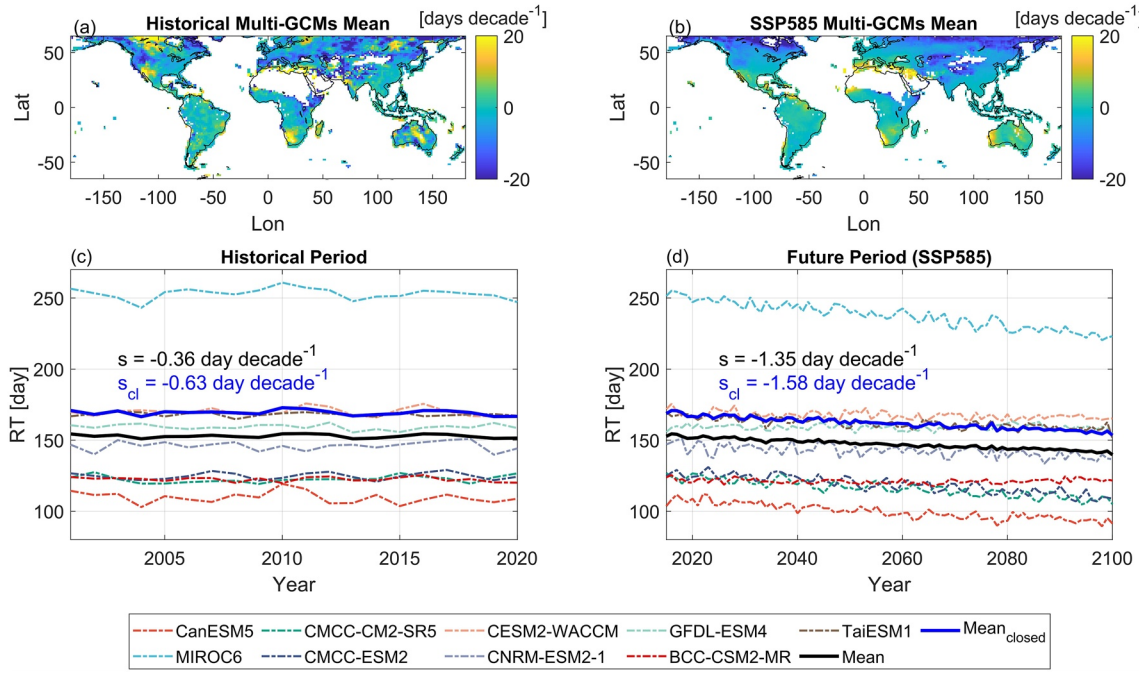

Figure 4. Spatial patterns and temporal trends of soil water RT from CMIP6 simulations under historical and SSP 585 scenarios. The maps show the spatial distribution of the trends in RT for the multi-GCMs mean with closed mass budget under the (a) historical and (b) SSP 585 scenarios. Areas with PR below 100 mm/year and tails of the RT distributions beyond 1%–99% are excluded. The dashed lines in the time series display the annual mean RT for the different GCMs at a global scale under the historical (c) and SSP 585 scenarios (d), and the thick black and blue line represents the average RT of the nine different GCMs and of the five models with closed mass budget, respectively. The term s represents the slope of the linear regression. The s without subscripts represents slope calculated based on all nine models, and with subscript cl refers to the results calculated for the five models with closed mass budget. The *p*-value for historical RT timeseries is larger than 0.05, while it is smaller than 0.05 under SSP 585 scenario.

statistically significant ($p = 0.006 < 0.05$) downward trend with a rate of −2.30 days decade^{-1} (−6.8 days °C^{-1}) in the period 2001 to 2020 (Figure 3c).

3.3. Historical and Future Trends in Soil Water RT in the CMIP6 Simulations

The simulations of nine GCMs (Table 1) show varying levels of SM and soil water RT averaged over the period from 2015 to 2100 (Figures S12 and S13 in Supporting Information S1). Despite noticeable differences across models, all models projected a significant increasing trend in global terrestrial ET and PR, with an average ET increase of 6.0 mm yr^{-1} decade^{-1} and an average PR increase of 7.9 mm yr^{-1} decade^{-1} (Figures S14a and S14b in Supporting Information S1). SM also displays a small (significant on the multi-model mean) decreasing trend despite substantial differences in the average SM among GCMs (Figure S14c in Supporting Information S1).

Under the future scenario, the distribution of changes in ET and PR in the northern and southern hemispheres is considerably different: PR and ET mostly increase in the northern hemisphere, while they decrease in most regions in the southern hemisphere (Figure S15, Table S3 in Supporting Information S1). SM decreases in most of the global latitudinal belts under the future scenarios albeit by a small percentage, similar to the changes in the historical periods. The change in RT is greatly influenced by changes in PR and ET, with the maximum increase in RT of 4.3% occurring between 25° and 35°S (Table S4 in Supporting Information S1) where PR and ET decrease the greatest (−2.3% and −2.1%, respectively), and the area with the largest decrease in RT is between 65° and 55°N with a change of −19.3%, which is also the region with the greatest increase in PR and ET (15.6% and 19.9%, respectively).

The temporal analysis of the RT changes in the CMIP6 historical simulation reaffirms that the terrestrial water cycle was accelerating at a global scale from 2001 to 2020, as RT was simulated to decrease at a rate of 0.36 days decade^{-1} (Figures 4a and 4c), even though the rate is smaller than found in the reanalysis data and the percentages of areas with accelerating/decelerating RT trends differ (Table 2). The spatial distribution of RT

changes as simulated in the CMIP6 historical periods is reasonably similar to the pattern observed with reanalysis. The acceleration of RT was evident at high latitudes and equatorial regions in the Northern Hemisphere. However, some discrepancies exist in certain regions, such as in the mid-west of Australia (Figures 3b and 4a). The comparison between the historical simulation and SSP 585 indicate that the terrestrial water cycle would continue to accelerate under this future emission pathways with RT decreasing at a higher rate of −1.35 days decade^{-1}. The RT changes expressed as the response of RT to changes in global mean land temperature are −1.1 and −2.2 days °C^{-1} for historical simulations and SSP 585 scenarios, respectively, remarking a stronger acceleration in the future scenarios. The multi-model mean of annual RT was 153 days (169 days for models with fully closed mass budget) from 2001 to 2020 and 143 days (157 days for models with fully closed mass budget) under the SSP 585 scenario for the period 2081–2100. The nine GCMs show a similar spatial pattern of changes in RT over the future period. The mean of models with closed mass budget under SSP 585 is shown in Figure 4b. Single models are shown in Figure S16 in Supporting Information S1, the distributions of RT changes are in Figure S17 in Supporting Information S1, and the corresponding distributions of RTs globally and for latitudinal bands are shown in Figure S18 in Supporting Information S1. Table S5 and S6 in Supporting Information S1 are reporting statistics for the different GCM models. We calculated the percentage of regions with accelerated hydrological cycle globally and under different latitudinal bands by averaging the results of the nine climate models, which showed that—at a global scale (65°N–65°S)—64.3%/35.7% regions are expected to accelerate/decelerate their terrestrial hydrological cycle during the period of 2015–2100, and 45.3% of the total analyzed land area shows a statistically significant acceleration, while 19.3% of the land area shows a significant decelerating trend.

The northern and southern hemispheres exhibit distinct spatial heterogeneity in the rate of the terrestrial water cycle change under future scenario. More than half of the northern hemisphere regions shows an accelerating trend (80.2% for 65°–23°N and 56.3% for 23°N–0°), while more than half of the southern hemisphere land area shows a decelerating trend (54.9% for 0°–23°S and 57.0% for 23°–65°S). The RT annual average, maximum, and minimum values for individual models are detailed in Table S7 in Supporting Information S1. The percentage of regions in different latitudinal zones with significant changes are listed in Table 2 (multi-model mean) and Tables S8 and S9 (single-models) in Supporting Information S1.

Changes in PR and ET are highly correlated with each other, and it is a priori difficult to disentangle which is the dominant control for changes in RT. Hence, we performed a Spearman's semi-partial correlation analysis (Padrón et al., 2017) between the grid-level RT variations and the corresponding changes in ET (Figure S19 in Supporting Information S1) and PR (Figure S20 in Supporting Information S1) for each of the nine GCMs in order to analyze the most influential factor leading to the change in RT. We performed the semi-partial correlation analysis on the difference in the mean values of the variables between the periods 2015–2045 and 2070–2100. As expected, changes in RT showed significant negative correlations with changes in both PR and ET. An increase in ET or PR can both reduce the soil water RT and thereby accelerate the terrestrial water cycle. However, the semi-partial correlation analysis suggests that changes in PR play a more dominant role in accelerating the terrestrial water cycle compared to changes in ET. The squared semi-partial correlation coefficient between the changes in RT and the change in PR is indeed greater ($\rho^2 = 0.14$, $\rho = -0.37$) than that for the changes in ET ($\rho^2 = 0.03$, $\rho = -0.17$) (Figure 5).

3.4. Controls in the Acceleration of the Terrestrial Water Cycle

To gain further insights into the effects of different climate variables on the acceleration of the terrestrial water cycle under future climate change scenarios, we run a number of simulations with the mechanistic ecohydrological model T&C to separate the effects of changing meteorological conditions (air temperature, atmospheric CO_2 concentration and PR) on the changes in RT. Despite the spatial mismatch, we still found a good correlation between the historical RT at the same 118 sites worldwide calculated with the ERA5 reanalysis product and the T&C simulations ($R^2 = 0.37$, Figure S21 in Supporting Information S1), which represent the land-surface and hydrological cycle in more detail and allow to mechanistically investigate the drivers of changes in soil water RT.

As changes in photosynthesis (GPP) and evapotranspiration (ET) caused by climate change are vital to quantify its effects on the hydrological and carbon cycle and provision of ecosystem services (Smallman & Williams, 2019; Y. Yang et al., 2016), we analyzed correlations between changes in soil water RT and changes in ET and GPP for the different climate perturbation scenarios, as listed in Table 3. The results show that a perturbation of ±15% in mean PR leads to the largest changes in RT, +11.23 days for decreased PR, which decelerates the terrestrial hydrological cycle, and −8.89 days for increased PR, which instead accelerates it. A perturbation of +250 ppm in

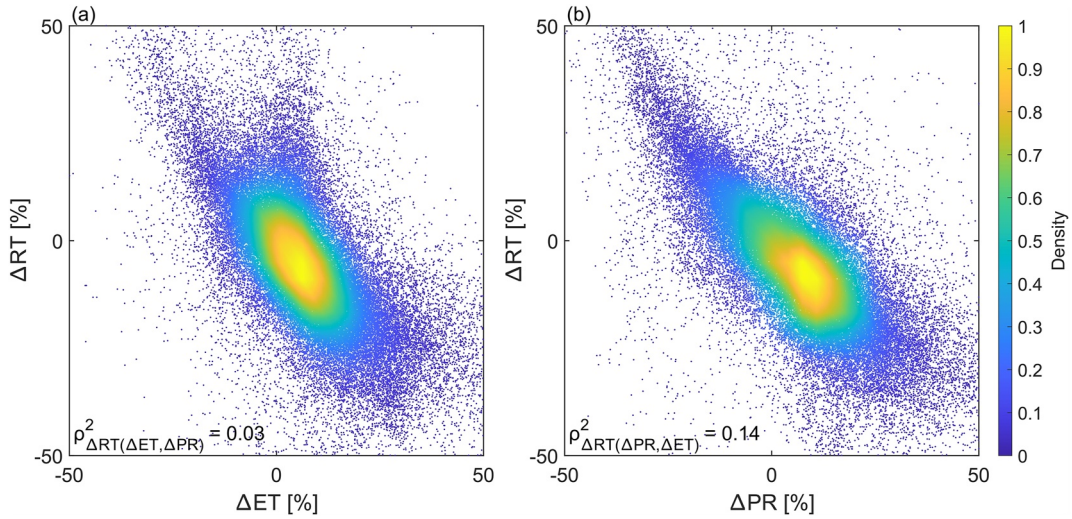

Figure 5. The density scatter plot depicts the semi-partial correlation between changes in RT and changes in the two main hydrological variables: ET (a) and PR (b). The scatter plots were obtained by combining simulations from nine GCMs. Changes in ET, PR and RT are defined as the difference between the annual means of PR, ET and RT for the periods 2015–2045 and 2070–2100. The term ρ^2 is the squared semi-partial correlation coefficient. The tails of the RT distributions beyond 1%–99% and values in the arid regions are excluded from the analysis. The subscript ΔRT (ΔET, ΔPR) represents the correlation between ΔET and ΔRT after the influence of variable ΔPR is removed from ΔRT, ΔRT (ΔPR, ΔET) represents the correlation between ΔPR and ΔRT after the influence of variable ΔET is removed from ΔRT.

atmospheric CO_2 results in a +3.11 days change in RT, mostly generated by reduced evapotranspiration and soil moisture savings induced by stomatal closure (Fatichi et al., 2016; Medlyn et al., 2001).

The results of the numerical experiments further showed that increased temperature and increased PR can shorten soil water RTs at most sites (Figures 6a and 6d), while increased CO_2 and reduced PR mostly lengthen RTs (Figures 6b and 6c). The effects of temperature and CO_2 largely compensate for each other as highlighted by experiments where combinations of the two perturbations are analyzed. For instance, if the CO_2 concentration is increased by 250 ppm (Figures 6e, 6f, and 6g) and the average temperature rises gradually by 1.5, 3.0 and 4.5°C, the decrease in RT caused by elevated temperature above 1.5°C can offset the deceleration effects caused by increased CO_2, thereby resulting in a lack of change in RT (ΔRT < 1 day). Similarly, if we fix temperature rise at +3°C (Figures 6f and 6h), and we decrease the rise of CO_2 from 250 to 150 ppm, we change the sign of the average ΔRT from an increase at CO_2 + 250 ppm to a decrease at CO_2 + 150 ppm. However, also in this case changes are relatively small (ΔRT < 1 day), when compared with changes induced by variations in PR or temperature and CO_2 alone. The detailed results of the changes in the variables under the 8 different perturbed scenarios can be found in the supplementary materials (Table S2 in Supporting Information S1).

Table 3
Results of the Numerical Experiments With T&C and Coefficients of Determination of the Relationship Between RT Changes and Changes in ET and GPP

Scenarios	Median ΔRT [days]	Correlation between ΔRT and ΔET [R^2]	Correlation between ΔRT and ΔGPP [R^2]
T_A + 3°C	−1.92	0.30 (−)	0.27 (−)
CO_2 + 250 ppm	3.11	0.11 (−)	0.07 (+)
PR − 15%	11.23	0.29 (+)	0.21 (+)
PR + 15%	−8.89	0.23 (+)	0.37 (+)
T_A + 1.5°C & CO_2 + 250 ppm	1.65	0.43 (−)	0.27 (−)
T_A + 3°C & CO_2 + 250 ppm	0.59	0.30 (−)	0.25 (−)
T_A + 4.5°C & CO_2 + 250 ppm	−0.24	0.31 (−)	0.28 (−)
T_A + 3°C & CO_2 + 150 ppm	−0.45	0.22 (−)	0.18 (−)

Note. The median soil water RTs is computed using 118 sites spanning various hydroclimatic, soil, and vegetation conditions. The Δ denotes the difference between perturbed and control simulations. The (+) and (−) represent positive correlation and negative correlation, respectively.

Under realistic future climate change scenarios, temperature and CO_2 are expected to increase, while changes in PR have a much higher uncertainty at the local scale than globally (Allan et al., 2014; Chadwick et al., 2013). ET is mostly increased by a positive change in temperature and decreased by higher CO_2 concentration (Figures 6a and 6b). Changes in PR lead to a positive correlation between changes in soil water RT and changes in ET (Figures 6c and 6d) as they largely determine the sign of the RT and ET change, while increases in temperature and CO_2 provides a negative correlation between changes in RT and changes in ET (Figures 6a, 6b, 6e, 6f, 6g, and 6h), as now RT changes are driven by ET changes.

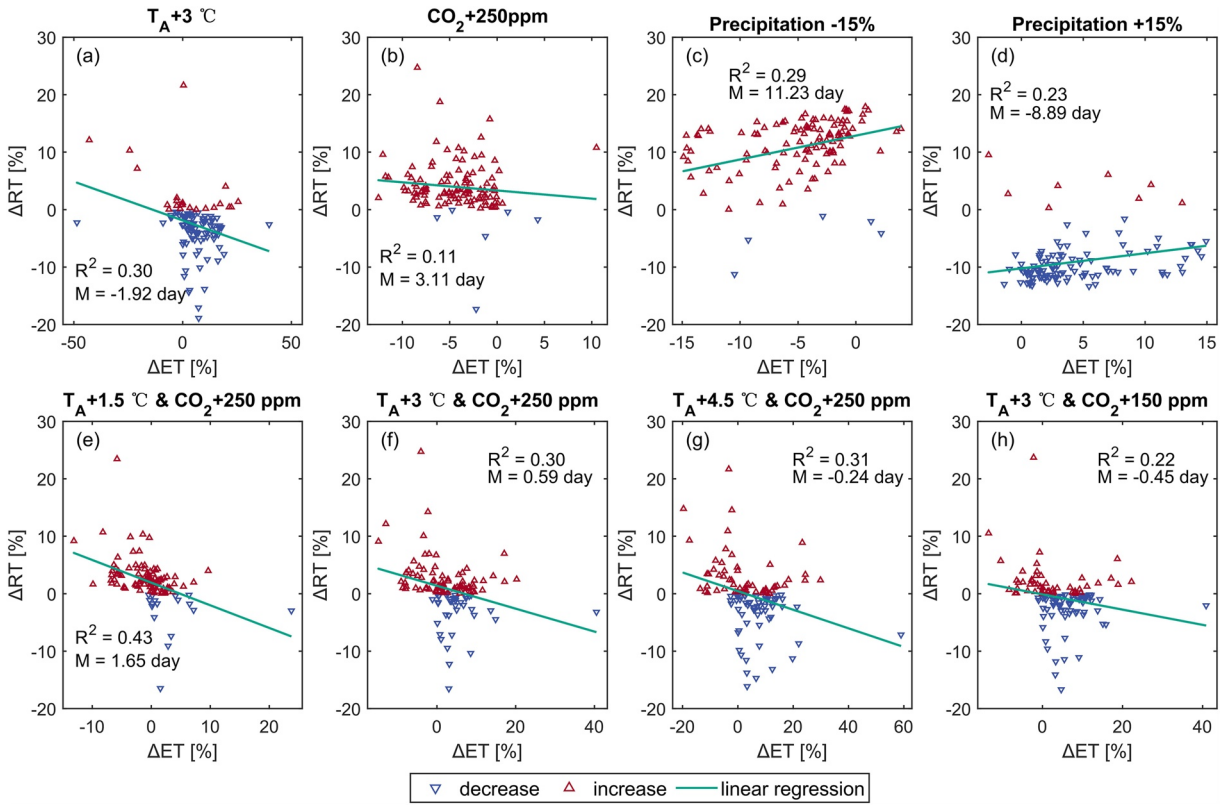

Figure 6. The scatter plots show the correlation between changes in RT and changes in ET under eight different climate perturbation scenarios simulated with the T&C model. The changes are defined as the difference between perturbed scenarios and control scenarios. The perturbed conditions include a temperature rise of 3°C (a), a 250 ppm increase in CO_2 (b), a 15% reduction in PR (c), a 15% increase in PR (d), a temperature rise by 1.5°C and a 250 ppm increase in CO_2 (e), a temperature rise by 3°C and a 250 ppm increase in CO_2 (f), a temperature rise by 4.5°C and a 250 ppm increase in CO_2 (g), and a temperature rise by 3°C and a 150 ppm increase in CO_2 (h). The red triangles refer to sites with an increase in RT and blue triangles representing sites which experience a decrease in RT due to the perturbation. The green lines depict the fitted linear regressions. R^2 is the coefficient of determination and M is the median change in RT in the 118 sites.

The correlation between GPP changes and RT changes (Figure S22 in Supporting Information S1) show similar patterns to the correlation of ET changes with RT changes as discussed above due to the strong coupling between photosynthesis and evapotranspiration, directly influenced by stomatal conductance, and indirectly affected by soil moisture content in the root zone. Elevated temperature, CO_2 and increased PR promoted photosynthetic activity in most of the simulated ecosystems, leading to an increase in GPP (Figures S22a, S22b, and S22d in Supporting Information S1), which is consistent with literature (Campbell et al., 2017; Walker et al., 2021; Zhu et al., 2016). The correlation between changes in RT and changes in GPP is positive with increased CO_2 or PR (Figures S22b, S22c, and S22d in Supporting Information S1), whereas under warmer conditions this correlation is negative (Figure S22a in Supporting Information S1). An increase in PR (Figure S22d in Supporting Information S1) promotes a stronger correlation between changes in RT and changes in GPP ($R^2 = 0.37$), whereas this correlation is weaker ($R^2 = 0.07$) with increased CO_2 (Figure S22b in Supporting Information S1). These complex patterns of correlation between changes in a given driving variable, soil water RT, and GPP show that it is difficult to generalize how a change in soil water RT itself will affect the vegetation productivity as changes in soil water RTs are co-occurring with other ecohydrological changes affecting GPP rather than driving them.

4. Discussion

4.1. RTs of Soil Water Is Decreasing Historically and Is Projected to Continue in the Future but With Significant Spatial Heterogeneities

We find an accelerating trend in the top meter soil water cycle at the global scale (after removing high-latitude regions, arid areas and RT distribution tails) characterized by a decrease in the soil water RT of −2.30 and −0.36 days decade^{-1} computed over the historical period with reanalysis and CMIP6, respectively, which is

projected to continue in the future with a rate of -1.35 days decade^{-1} according to CMIP6 simulations under the emission scenario SSP 585. Multi-model RT trends range from -3.4 to 0.0 days decade^{-1} (Table S6 in Supporting Information S1) but this range might underestimate the true uncertainty. Given the considerable underestimation of the RT trends from CMIP6 in the historical period of almost an order of magnitude, if this underestimation persists in the future, it is possible that the trend of -1.35 days decade^{-1} might be just a conservative estimate and larger RT changes might instead occur. The acceleration of the terrestrial water cycle has been analyzed in previous studies, some of which have derived acceleration by calculating changes in hydrological fluxes such as PR and ET (Durack et al., 2012; Huntington, 2006; Huntington et al., 2018). An accelerated water cycle may provide additional available renewable freshwater resources for regions with water scarcity issues through enhanced PR, although the enhancement of precipitation extremes and seasonal variations in the hydrological variables make this prediction uncertain (Oki & Kanae, 2006). Regional studies have found that the terrestrial water cycle in Illinois, USA, from 1983 to 2013 showed an accelerating trend (Yeh & Wu, 2018), and others illustrated that the terrestrial water cycle changes in Tibetan Plateau are mainly influenced by changes in surface runoff and soil moisture (J. Wang et al., 2020). Large scale analysis have corroborated these findings with data sets, such as the Gravity Recovery and Climate Experiment (GRACE), to reach similar conclusions (Eicker et al., 2016). However, a quantitative analysis of the hydrological cycle acceleration over land using multiple sources of information for present and future climate was lacking.

Here, we find that changes in RT are spatially heterogenous mainly due to the spatial heterogenous changes of the involved water fluxes. As there is a significant negative correlation between changes in PR, ET, and RT (Figure 5 for 65°N–65°S, Figure S23 in Supporting Information S1 for 23°N–23°S), this spatial heterogeneity is mostly dictated by the different patterns of changes in PR and ET, which are also strongly correlated to each other through mass conservation (Equation 1).

4.2. Drivers of Variation in RT Changes

The correlations between changes in ET and PR and ΔRT are both negative. The result of the semi-partial correlation analysis highlights that changes in PR are a much more dominant driver of the acceleration of the terrestrial water cycle than changes in ET, even though changes in the two variables are strongly correlated in many sites worldwide for obvious mass conservation reasons. The importance of PR variability in the study of the terrestrial water cycle is undoubtable (Giorgi et al., 2019; Mathew & Kumar, 2019; Trenberth et al., 2003; Trenberth & Zhang, 2018), but here we demonstrate that it is the main driver of the projected acceleration of the hydrological cycle, much more important than changes in ET associated with higher temperatures. Please note, though, that at the global scale changes in PR are a result of the overall global warming and thus indirectly related to temperature (e.g., Allan et al., 2014; Schneider et al., 2010). Previous studies have shown that absolute precipitation changes are higher in the tropics than in temperate regions (Lau et al., 2013). The specific regional distribution of RT reaffirms that PR is more essential than ET in driving the terrestrial water cycle speed: for example, in the latitudinal bands 35°–45°S and 45°–55°S, the future terrestrial water cycle decelerates with a 2.8% and 1.6% increase in RT, respectively. In terms of hydroclimatic variables, ET is projected to increase by 4.6% and 2.5% in these two regions, but PR is expected to decrease by 0.3% and 2.2% respectively in the future period (Table S4 in Supporting Information S1). The expected acceleration effect due to increased ET is therefore suppressed by the deceleration effect induced by reduced PR despite a greater relative magnitude of changes in ET, remarking how PR plays a more dominant role than ET in influencing changes of RT. Additionally, an ET increase can be also compensated by a decrease in LK, especially in water limited ecosystems, thus dampening the overall change in RT (Equation 5). It has also to be noticed that in all arid and semiarid ecosystems, changes in ET cannot be greater than changes in PR over the long period studied here, which limits the potential role of ET in comparison to PR in affecting RT (Table S4 in Supporting Information S1). However, on sub-annual time scales, other dynamics might occur as a change in ET, not even associated to PR, for example, during a heat wave, may likely lead to pronounced changes in RT for a short period of time.

Increased CO_2 and temperature have a compensating effect on changes in RT mainly because of their counteracting effects on ET. Higher temperatures tend to increase plant transpiration, while increased CO_2 reduces stomatal conductance and thus inhibits transpiration (Fatichi et al., 2021; Kirschbaum & McMillan, 2018; Manzoni et al., 2022). As evident from the numerical experiments, changes in RT in response to plausible changes in CO_2 and air temperature have a considerably lower magnitude than RT changes in response to plausible modifications

in PR (Figure 6 and Figure S22 in Supporting Information S1, Table 3). As the concurrent increases in air temperature and CO_2, which changes are strongly correlated (e.g., Seneviratne et al., 2016), tend to generate compensating effects on the changes in RTs, the ultimate net effect of these two variables is likely a very minor RT deviation from historical values in the absence of PR changes.

4.3. The Potential Effects of Changes in the Speed of the Terrestrial Water Cycle on Vegetation Productivity and Soil Biogeochemistry

Beyond its theoretical importance, changes in soil water RT can modify plant activity and ecosystem functioning. Soil water RT affects plants by modifying the amount of time roots have on average to uptake nutrients from the soil (Carminati et al., 2010; Comas et al., 2010; Hinsinger et al., 2009; Smettem, 1984). Concurrently, soil microbial activity is also likely influenced by changes in soil water RT and can modify the rate of soil organic matter processing, thus feeding back on plant mineral nutrition and affecting carbon storage capabilities (Manzoni et al., 2012; Moyano et al., 2013). Under the scenarios projected in this study, the global average RT of soil water is expected to decrease at a rate of -1.35 days decade $^{-1}$ (-0.9% decade^{-1}) in the rest of the 21st century with an approximately linear rate, meaning that the average contact time between soil and water will be shorter in the future by several days in many locations on Earth. Overall changes in GPP are predominantly affected by changes in the meteorological variables and correlations between changes in GPP and RT are complex and not particularly strong (Figure S22 in Supporting Information S1), as higher PR might stimulate vegetation productivity even when RTs are reduced, and conversely lower PR might reduce GPP, while increasing RTs. However, the accelerated soil water cycle may have detrimental effects for specific plant species or alter microbial dynamics with implications still to be determined. In addition, as water is a solvent for chemical reactions, changes in RT can have an impact on the lateral and vertical transport of nutrients and solutes over the vadose zone (e.g., Botter et al., 2020; Nielsen et al., 1986; Rinaldo et al., 2015) with consequences for stream water quality, even though RTs below 1 m soil depth and in the groundwater can be longer or much longer than in the top meter of soil and thus the effects of RT changes in the top-soil should be dampened with depth.

4.4. Limits of Interpretation

Changes in temperature, PR and carbon dioxide are analyzed explicitly here with numerical experiments using an ecohydrological model and the overall impact of climate change is analyzed using CMIP6 simulations. However, other anthropogenic interventions including land cover changes and vegetation changes are only partially included in the models used in the CMIP6 simulations and in the T&C simulations (e.g., vegetation responds to climate, but without land use shifts). Additional anthropogenic interventions for example, field drainage or urbanization, are expected to further modify soil water RT, but they are likely local and not accounted for in our study. An additional source of uncertainty is the variability among projections obtained with different GCMs, especially considering that the mass budget is not perfectly preserved in some of them (Figure S2 in Supporting Information S1) and that they also have different spatial resolutions. However, differences among GCMs are affecting more the magnitude of RTs and RT changes rather than the overall spatial pattern (Figures S15 and S16 in Supporting Information S1) or future trajectory (Figure 4) and despite non negligible differences all models are projecting a decrease in RT in the future (Table S6 in Supporting Information S1) and a larger area with accelerating rather than decelerating trends (Table S9 in Supporting Information S1). Therefore, despite the existing uncertainties the overall main conclusion of the terrestrial hydrological cycle accelerating on average, but with large spatial heterogeneities, is robust to differences among climate models.

The correlations between changes in soil water RT and GPP were not very strong ($R^2 < 0.37$) and of variable sign based on the perturbed meteorological variables (Figure S22 in Supporting Information S1), which suggests that there is not a simple relationship between changes in vegetation productivity and RT across ecosystems globally. Therefore, the discussion of potential impacts of changes in RT needs to be associated to a specific driver (e.g., temperature, CO_2, or precipitation) and requires specific site level analyses. Additionally, the change in the variables selected for the climate perturbation experiment is somehow arbitrary and it only approximates potential climatic changes expected in the future (e.g., Song et al., 2019), and it does not include large scale feedbacks. However, this analysis is only done to highlight mechanistic controls. The discussion of actual projections is based on the CMIP6 results, which instead include all known climate feedbacks triggered by the increase in greenhouse gases. Furthermore, we arbitrary selected the first meter of soil to analyze changes in the velocity

of the terrestrial water cycle. While RT in the top 1 m soil column correlates well with RT calculated with 0.1 and 2 m deep soil columns, an analysis of deep-water storages (Fan et al., 2013; McCormick et al., 2021) might complicate the picture and include additional hydrogeological controls, which can be explored in the future. When we compared the change in RT between the historical period and the future period, we applied two different methods to calculate the RT depending on the data set because the data for LK is missing in the reanalysis product, which results in a less precise comparison even though results from the two computation methods are shown to be highly correlated.

5. Conclusions

This article determines if the terrestrial water cycle is accelerating over land by calculating changes in the average soil water RT in the top meter of soil. In the analyzed area (65°N–65°S, excluding deserts and distribution tails), the annual mean RT was 136 days during the historical period (2001–2020) and 55.8% of the study area showed an accelerating trend in the terrestrial water cycle over the last two decades using reanalysis and according to the projections of the CMIP6 GCMs the area with accelerating terrestrial hydrological cycle will even increase in the future (64.3%). There are important geographical differences in the trends of soil water RT with the strongest trends found at high latitudes in the northern hemisphere and with the southern hemisphere showing deceleration rather than acceleration of the water cycle in the soil with higher RTs. However, on a global average a RT change of −2.30 and −0.36 days decade^{-1} from 2001 to 2020 was computed using reanalysis and the CMIP6 historical scenarios, respectively. This trend is projected to continue over a much longer period (2015–2100) at a rate of −1.35 days decade^{-1} under the SSP 585 future climate scenario. These RT changes expresses per degree of global warming over land are −1.1 and −2.2 days °C^{-1} using CMIP6 historical and SSP 585 scenarios. Changes in PR are shown to play a more dominant role than changes in ET in driving the acceleration and deceleration of the terrestrial water cycle. This is confirmed by targeted numerical experiments with a mechanistic ecohydrological model. Furthermore, changes induced by increased temperature and CO_2 play in opposite directions and tend to largely compensate for each other. In summary, we brought various lines of evidence and process-based explanations for an increase in the speed of the hydrological cycle over land in the historical period which based on drivers and mechanistic understanding is likely to continue in the coming future and projected to do so by GCMs. This knowledge complements the more documented acceleration of the atmospheric hydrological cycle (Allan et al., 2014; Ohmura & Wild, 2002), highlighting a much larger spatial heterogeneity over land.

Data Availability Statement

Publicly available data was used in this study. Reanalysis data is available at https://www.ecmwf.int/en/era5-land. CMIP6 model outputs can be obtained from https://esgf-node.llnl.gov/search/cmip6/. The T&C model code can be found at https://doi.org/10.24433/CO.0905087.v2.

Acknowledgments
This study was supported by the National University of Singapore (Singapore Ministry of Education Academic Research Fund Tier 1) through the project "Bridging scales from below: The role of heterogeneities in the global water and carbon budgets" Award Number: 22-3637-A0001.

References

Allan, R. P., Liu, C., Zahn, M., Lavers, D. A., Koukouvagias, E., & Bodas-Salcedo, A. (2014). Physically consistent responses of the global atmospheric hydrological cycle in models and observations. *Surveys in Geophysics*, *35*(3), 533–552. https://doi.org/10.1007/s10712-012-9213-z

Almazroui, M., Ashfaq, M., Islam, M. N., Rashid, I. U., Kamil, S., Abid, M. A., et al. (2021). Assessment of CMIP6 performance and projected temperature and precipitation changes over South America. *Earth Systems and Environment*, *5*(2), 155–183. https://doi.org/10.1007/s41748-021-00233-6

Anav, A., Friedlingstein, P., Beer, C., Ciais, P., Harper, A., Jones, C., et al. (2015). Spatiotemporal patterns of terrestrial gross primary production: A review: GPP spatiotemporal patterns. *Reviews of Geophysics*, *53*(3), 785–818. https://doi.org/10.1002/2015RG000483

Arias, P. A., Bellouin, N., Coppola, E., Jones, R. G., Krinner, G., Marotzke, J., et al. (2021). Technical summary. In V. P. Zhai, A. Pirani, S. L. Connors, C. Péan, S. Berger, N. Caud, Y. Chen, L. Goldfarb, M.I. Gomis, M. Huang, K. Leitzell, E. Lonnoy, J.B.R. Matthews, T.K. Maycock, T. Waterfield, O. Yelekçi, R. Yu, & B. Zhou (Eds.), *Climate change 2021: The physical science basis. Contribution of working group I to the sixth assessment report of the intergovernmental panel on climate change [Masson-Delmotte* (pp. 33–144). Cambridge University Press. https://doi.org/10.1017/9781009157896.002

Assouline, S., & Or, D. (2013). Conceptual and parametric representation of soil hydraulic properties: A review. *Vadose Zone Journal*, *12*(4), 1–20. https://doi.org/10.2136/vzj2013.07.0121

Bateni, S. M., & Entekhabi, D. (2012). Relative efficiency of land surface energy balance components. *Water Resources Research*, *48*(4). https://doi.org/10.1029/2011WR011357

Berg, A., Findell, K., Lintner, B., Giannini, A., Seneviratne, S. I., van den Hurk, B., et al. (2016). Land–atmosphere feedbacks amplify aridity increase over land under global warming. *Nature Climate Change*, *6*(9), 869–874. https://doi.org/10.1038/nclimate3029

Bickel, S., & Or, D. (2020). Soil bacterial diversity mediated by microscale aqueous-phase processes across biomes. *Nature Communications*, *11*(1), 116. https://doi.org/10.1038/s41467-019-13966-w

Botter, M., Li, L., Hartmann, J., Burlando, P., & Fatichi, S. (2020). Depth of solute generation is a dominant control on concentration-discharge relations. *Water Resources Research*, *56*(8). https://doi.org/10.1029/2019WR026695

Botter, M., Zeeman, M., Burlando, P., & Fatichi, S. (2021). Impacts of fertilization on grassland productivity and water quality across the European Alps under current and warming climate: Insights from a mechanistic model. *Biogeosciences*, *18*(6), 1917–1939. https://doi.org/10.5194/bg-18-1917-2021

Brümmer, C., Black, T. A., Jassal, R. S., Grant, N. J., Spittlehouse, D. L., Chen, B., et al. (2012). How climate and vegetation type influence evapotranspiration and water use efficiency in Canadian forest, peatland and grassland ecosystems. *Agricultural and Forest Meteorology*, *153*, 14–30. https://doi.org/10.1016/j.agrformet.2011.04.008

Brutsaert, W. (2005). *Hydrology: An introduction*. Cambridge university press.

Byrne, M. P., & O'Gorman, P. A. (2015). The response of precipitation minus evapotranspiration to climate warming: Why the "Wet-Get-Wetter, Dry-Get-Drier" scaling does not hold over land. *Journal of Climate*, *28*(20), 8078–8092. https://doi.org/10.1175/JCLI-D-15-0369.1

Campbell, J. E., Berry, J. A., Seibt, U., Smith, S. J., Montzka, S. A., Launois, T., et al. (2017). Large historical growth in global terrestrial gross primary production. *Nature*, *544*(7648), 84–87. https://doi.org/10.1038/nature22030

Carminati, A., Moradi, A. B., Vetterlein, D., Vontobel, P., Lehmann, E., Weller, U., et al. (2010). Dynamics of soil water content in the rhizosphere. *Plant and Soil*, *332*(1–2), 163–176. https://doi.org/10.1007/s11104-010-0283-8

Cavagnaro, T. R. (2016). Soil moisture legacy effects: Impacts on soil nutrients, plants and mycorrhizal responsiveness. *Soil Biology and Biochemistry*, *95*, 173–179. https://doi.org/10.1016/j.soilbio.2015.12.016

Chadwick, R., Boutle, I., & Martin, G. (2013). Spatial patterns of precipitation change in CMIP5: Why the rich do not get richer in the tropics. *Journal of Climate*, *26*(11), 3803–3822. https://doi.org/10.1175/JCLI-D-12-00543.1

Chen, D., Rojas, M., Samset, B. H., Cobb, K., Diongue Niang, A., Edwards, P., et al. (2021). Framing, context, and methods. In P. Zhai, A. Pirani, S. L. Connors, C. Péan, S. Berger, N. Caud, Y. Chen, L. Goldfarb, M.I. Gomis, M. Huang, K. Leitzell, E. Lonnoy, J.B.R. Matthews, T.K. Maycock, T. Waterfield, O. Yelekçi, R. Yu, & B. Zhou (Eds.), *Climate change 2021: The physical science basis. Contribution of working group I to the sixth assessment report of the intergovernmental panel on climate change [Masson-Delmotte, V.]* (pp. 147–286). Cambridge University Press. https://doi.org/10.1017/9781009157896.003

Comas, L. H., Bauerle, T. L., & Eissenstat, D. M. (2010). Biological and environmental factors controlling root dynamics and function: Effects of root ageing and soil moisture. *Australian Journal of Grape and Wine Research*, *16*, 131–137. https://doi.org/10.1111/j.1755-0238.2009.00078.x

Dingman, S. L. (2015). *Physical hydrology* (p. 24). Waveland press.

Durack, P. J., Wijffels, S. E., & Matear, R. J. (2012). Ocean salinities reveal strong global water cycle intensification during 1950 to 2000. *Science*, *336*(6080), 455–458. https://doi.org/10.1126/science.1212222

Eicker, A., Forootan, E., Springer, A., Longuevergne, L., & Kusche, J. (2016). Does GRACE see the terrestrial water cycle "intensifying". *Journal of Geophysical Research: Atmospheres*, *121*(2), 733–745. https://doi.org/10.1002/2015JD023808

Eyring, V., Bony, S., Meehl, G. A., Senior, C. A., Stevens, B., Stouffer, R. J., & Taylor, K. E. (2016). Overview of the Coupled Model Intercomparison Project Phase 6 (CMIP6) experimental design and organization. *Geoscientific Model Development*, *9*(5), 1937–1958. https://doi.org/10.5194/gmd-9-1937-2016

Fan, Y., Li, H., & Miguez-Macho, G. (2013). Global patterns of groundwater table depth. *Science*, *339*(6122), 940–943. https://doi.org/10.1126/science.1229881

Fan, Y., Miguez-Macho, G., Jobbágy, E. G., Jackson, R. B., & Otero-Casal, C. (2017). Hydrologic regulation of plant rooting depth. *Proceedings of the National Academy of Sciences*, *114*(40), 10572–10577. https://doi.org/10.1073/pnas.1712381114

Fatichi, S., Peleg, N., Mastrotheodoros, T., Pappas, C., & Manoli, G. (2021). An ecohydrological journey of 4500 years reveals a stable but threatened precipitation–groundwater recharge relation around Jerusalem. *Science Advances*, *7*(37), eabe6303. https://doi.org/10.1126/sciadv.abe6303

Fatichi, S., Ivanov, V. Y., & Caporali, E. (2012a). A mechanistic ecohydrological model to investigate complex interactions in cold and warm water-controlled environments: 1. Theoretical framework and plot-scale analysis. *Journal of Advances in Modeling Earth Systems*, *4*(2). https://doi.org/10.1029/2011MS000086

Fatichi, S., Ivanov, V. Y., & Caporali, E. (2012b). A mechanistic ecohydrological model to investigate complex interactions in cold and warm water-controlled environments: 2. Spatiotemporal analyses. *Journal of Advances in Modeling Earth Systems*, *4*(2). https://doi.org/10.1029/2011MS000087

Fatichi, S., Leuzinger, S., Paschalis, A., Langley, J. A., Donnellan Barraclough, A., & Hovenden, M. J. (2016). Partitioning direct and indirect effects reveals the response of water-limited ecosystems to elevated CO_2. *Proceedings of the National Academy of Sciences*, *113*(45), 12757–12762. https://doi.org/10.1073/pnas.1605036113

Fatichi, S., & Pappas, C. (2017). Constrained variability of modeled *T: ET* ratio across biomes: Transpiration:evapotranspiration ratio. *Geophysical Research Letters*, *44*(13), 6795–6803. https://doi.org/10.1002/2017GL074041

Fatichi, S., Zeeman, M. J., Fuhrer, J., & Burlando, P. (2014). Ecohydrological effects of management on subalpine grasslands: From local to catchment scale. *Water Resources Research*, *50*(1), 148–164. https://doi.org/10.1002/2013WR014535

Gerten, D., Schaphoff, S., Haberlandt, U., Lucht, W., & Sitch, S. (2004). Terrestrial vegetation and water balance—Hydrological evaluation of a dynamic global vegetation model. *Journal of Hydrology*, *286*(1–4), 249–270. https://doi.org/10.1016/j.jhydrol.2003.09.029

Giorgi, F., Raffaele, F., & Coppola, E. (2019). The response of precipitation characteristics to global warming from climate projections. *Earth System Dynamics*, *10*(1), 73–89. https://doi.org/10.5194/esd-10-73-2019

Greve, P., Orlowsky, B., Mueller, B., Sheffield, J., Reichstein, M., & Seneviratne, S. I. (2014). Global assessment of trends in wetting and drying over land. *Nature Geoscience*, *7*(10), 716–721. https://doi.org/10.1038/ngeo2247

Greve, P., & Seneviratne, S. I. (2015). Assessment of future changes in water availability and aridity. *Geophysical Research Letters*, *42*(13), 5493–5499. https://doi.org/10.1002/2015GL064127

Haddeland, I., Lettenmaier, D. P., & Skaugen, T. (2006). Effects of irrigation on the water and energy balances of the Colorado and Mekong river basins. *Journal of Hydrology*, *324*(1–4), 210–223. https://doi.org/10.1016/j.jhydrol.2005.09.028

Held, I. M., & Soden, B. J. (2006). Robust responses of the hydrological cycle to global warming. *Journal of Climate*, *19*(21), 5686–5699. https://doi.org/10.1175/JCLI3990.1

Hersbach, H., Bell, B., Berrisford, P., Hirahara, S., Horányi, A., Muñoz-Sabater, J., et al. (2020). The ERA5 global reanalysis. *Quarterly Journal of the Royal Meteorological Society*, *146*(730), 1999–2049. https://doi.org/10.1002/qj.3803

Hinsinger, P., Bengough, A. G., Vetterlein, D., & Young, I. M. (2009). Rhizosphere: Biophysics, biogeochemistry and ecological relevance. *Plant and Soil*, *321*(1–2), 117–152. https://doi.org/10.1007/s11104-008-9885-9

Hirschi, M., Mueller, B., Dorigo, W., & Seneviratne, S. I. (2014). Using remotely sensed soil moisture for land–atmosphere coupling diagnostics: The role of surface vs. root-zone soil moisture variability. *Remote Sensing of Environment*, *154*, 246–252. https://doi.org/10.1016/j.rse.2014.08.030

Humphrey, V., Berg, A., Ciais, P., Gentine, P., Jung, M., Reichstein, M., et al. (2021). Soil moisture–atmosphere feedback dominates land carbon uptake variability. *Nature*, *592*(7852), 65–69. https://doi.org/10.1038/s41586-021-03325-5

Huntington, T. G. (2006). Evidence for intensification of the global water cycle: Review and synthesis. *Journal of Hydrology*, *319*(1–4), 83–95. https://doi.org/10.1016/j.jhydrol.2005.07.003

Huntington, T. G., Weiskel, P. K., Wolock, D. M., & McCabe, G. J. (2018). A new indicator framework for quantifying the intensity of the terrestrial water cycle. *Journal of Hydrology*, *559*, 361–372. https://doi.org/10.1016/j.jhydrol.2018.02.048

Jackson, R. B., Canadell, J., Ehleringer, J. R., Mooney, H. A., Sala, O. E., & Schulze, E. D. (1996). A global analysis of root distributions for terrestrial biomes. *Oecologia*, *108*(3), 389–411. https://doi.org/10.1007/bf00333714

Jung, M., Reichstein, M., Ciais, P., Seneviratne, S. I., Sheffield, J., Goulden, M. L., et al. (2010). Recent decline in the global land evapotranspiration trend due to limited moisture supply. *Nature*, *467*(7318), 951–954. https://doi.org/10.1038/nature09396

Katul, G. G., Oren, R., Manzoni, S., Higgins, C., & Parlange, M. B. (2012). Evapotranspiration: A process driving mass transport and energy exchange in the soil-plant-atmosphere-climate system. *Reviews of Geophysics*, *50*(3). https://doi.org/10.1029/2011RG000366

Kaur, S., Kaur, R., & Chauhan, B. S. (2018). Understanding crop-weed-fertilizer-water interactions and their implications for weed management in agricultural systems. *Crop Protection*, *103*, 65–72. https://doi.org/10.1016/j.cropro.2017.09.011

Kirschbaum, M. U. F., & McMillan, A. M. S. (2018). Warming and elevated CO_2 have opposing influences on transpiration. Which is more important? *Current Forestry Reports*, *4*(2), 51–71. https://doi.org/10.1007/s40725-018-0073-8

Lau, W. K.-M., Wu, H.-T., & Kim, K.-M. (2013). A canonical response of precipitation characteristics to global warming from CMIP5 models. *Geophysical Research Letters*, *40*(12), 3163–3169. https://doi.org/10.1002/grl.50420

Liu, J., You, Y., Li, J., Sitch, S., Gu, X., Nabel, J. E. M. S., et al. (2021). Response of global land evapotranspiration to climate change, elevated CO_2, and land use change. *Agricultural and Forest Meteorology*, *311*, 108663. https://doi.org/10.1016/j.agrformet.2021.108663

Manoli, G., Ivanov, V. Y., & Fatichi, S. (2018). Dry-season greening and water stress in Amazonia: The role of modeling leaf phenology. *Journal of Geophysical Research: Biogeosciences*, *123*(6), 1909–1926. https://doi.org/10.1029/2017JG004282

Manzoni, S., Fatichi, S., Feng, X., Katul, G. G., Way, D., & Vico, G. (2022). Consistent responses of vegetation gas exchange to elevated atmospheric CO_2 emerge from heuristic and optimization models. *Biogeosciences*, *19*(17), 4387–4414. https://doi.org/10.5194/bg-19-4387-2022

Manzoni, S., Schimel, J. P., & Porporato, A. (2012). Responses of soil microbial communities to water stress: Results from a meta-analysis. *Ecology*, *93*(4), 930–938. https://doi.org/10.1890/11-0026.1

Mastrotheodoros, T., Pappas, C., Molnar, P., Burlando, P., Keenan, T. F., Gentine, P., et al. (2017). Linking plant functional trait plasticity and the large increase in forest water use efficiency. *Journal of Geophysical Research: Biogeosciences*, *122*(9), 2393–2408. https://doi.org/10.1002/2017JG003890

Mathew, S. S., & Kumar, K. K. (2019). Characterization of the long-term changes in moisture, clouds and precipitation in the ascending and descending branches of the Hadley Circulation. *Journal of Hydrology*, *570*, 366–377. https://doi.org/10.1016/j.jhydrol.2018.12.047

McCormick, E. L., Dralle, D. N., Hahm, W. J., Tune, A. K., Schmidt, L. M., Chadwick, K. D., & Rempe, D. M. (2021). Widespread woody plant use of water stored in bedrock. *Nature*, *597*(7875), 225–229. https://doi.org/10.1038/s41586-021-03761-3

Medlyn, B. E., Barton, C. V. M., Broadmeadow, M. S. J., Ceulemans, R., Angelis, P. D., Forstreuter, M., et al. (2001). Stomatal conductance of forest species after long-term exposure to elevated CO_2 concentration: A synthesis. *New Phytologist*, *149*(2), 247–264. https://doi.org/10.1046/j.1469-8137.2001.00028.x

Moyano, F. E., Manzoni, S., & Chenu, C. (2013). Responses of soil heterotrophic respiration to moisture availability: An exploration of processes and models. *Soil Biology and Biochemistry*, *59*, 72–85. https://doi.org/10.1016/j.soilbio.2013.01.002

Muñoz-Sabater, J., Dutra, E., Agustí-Panareda, A., Albergel, C., Arduini, G., Balsamo, G., et al. (2021). ERA5-Land: A state-of-the-art global reanalysis dataset for land applications. *Earth System Science Data*, *13*(9), 4349–4383. https://doi.org/10.5194/essd-13-4349-2021

Nielsen, D. R., Van Genuchten, M., & Biggar, J. W. (1986). Water flow and solute transport processes in the unsaturated zone. *Water Resources Research*, *22*(9S), 89S–108S. https://doi.org/10.1029/WR022i09Sp0089S

Ohmura, A., & Wild, M. (2002). Is the hydrological cycle accelerating? *Science*, *298*(5597), 1345–1346. https://doi.org/10.1126/science.1078972

Oki, T., & Kanae, S. (2006). Global hydrological cycles and world water resources. *Science, New Series*, *313*(5790), 1068–1072. https://doi.org/10.1126/science.1128845

Ozdogan, M., Rodell, M., Beaudoing, H. K., & Toll, D. L. (2010). Simulating the effects of irrigation over the United States in a land surface model based on satellite-derived agricultural data. *Journal of Hydrometeorology*, *11*(1), 171–184. https://doi.org/10.1175/2009JHM1116.1

Padrón, R. S., Gudmundsson, L., Greve, P., & Seneviratne, S. I. (2017). Large-scale controls of the surface water balance over land: Insights from a systematic review and meta-analysis. *Water Resources Research*, *53*(11), 9659–9678. https://doi.org/10.1002/2017WR021215

Pan, S., Pan, N., Tian, H., Friedlingstein, P., Sitch, S., Shi, H., et al. (2020). Evaluation of global terrestrial evapotranspiration using state-of-the-art approaches in remote sensing, machine learning and land surface modeling. *Hydrology and Earth System Sciences*, *24*(3), 1485–1509. https://doi.org/10.5194/hess-24-1485-2020

Pappas, C., Fatichi, S., & Burlando, P. (2016). Modeling terrestrial carbon and water dynamics across climatic gradients: Does plant trait diversity matter? *New Phytologist*, *209*(1), 137–151. https://doi.org/10.1111/nph.13590

Paschalis, A., Bonetti, S., Guo, Y., & Fatichi, S. (2022). On the uncertainty induced by pedotransfer functions in terrestrial biosphere modeling. *Water Resources Research*, *58*(9). https://doi.org/10.1029/2021WR031871

Paschalis, A., Fatichi, S., Pappas, C., & Or, D. (2018). Covariation of vegetation and climate constrains present and future T/ET variability. *Environmental Research Letters*, *13*(10), 104012. https://doi.org/10.1088/1748-9326/aae267

Paschalis, A., Katul, G. G., Fatichi, S., Palmroth, S., & Way, D. (2017). On the variability of the ecosystem response to elevated atmospheric CO_2 across spatial and temporal scales at the Duke forest FACE experiment. *Agricultural and Forest Meteorology*, *232*, 367–383. https://doi.org/10.1016/j.agrformet.2016.09.003

Pokhrel, Y., Hanasaki, N., Koirala, S., Cho, J., Yeh, P. J.-F., Kim, H., et al. (2012). Incorporating anthropogenic water regulation modules into a land surface model. *Journal of Hydrometeorology*, *13*(1), 255–269. https://doi.org/10.1175/JHM-D-11-013.1

Popp, A., Calvin, K., Fujimori, S., Havlik, P., Humpenöder, F., Stehfest, E., et al. (2017). Land-use futures in the shared socio-economic pathways. *Global Environmental Change*, *42*, 331–345. https://doi.org/10.1016/j.gloenvcha.2016.10.002

Puma, M. J., & Cook, B. I. (2010). Effects of irrigation on global climate during the 20th century. *Journal of Geophysical Research*, *115*(D16), D16120. https://doi.org/10.1029/2010JD014122

Rinaldo, A., Benettin, P., Harman, C. J., Hrachowitz, M., McGuire, K. J., van der Velde, Y., et al. (2015). Storage selection functions: A coherent framework for quantifying how catchments store and release water and solutes. *Water Resources Research*, *51*(6), 4840–4847. https://doi.org/10.1002/2015WR017273

Robinson, D. A., Campbell, C. S., Hopmans, J. W., Hornbuckle, B. K., Jones, S. B., Knight, R., et al. (2008). Soil moisture measurement for ecological and hydrological watershed-scale observatories: A review. *Vadose Zone Journal*, *7*(1), 358–389. https://doi.org/10.2136/vzj2007.0143

Roderick, M. L., Sun, F., Lim, W. H., & Farquhar, G. D. (2014). A general framework for understanding the response of the water cycle to global warming over land and ocean. *Hydrology and Earth System Sciences*, *18*(5), 1575–1589. https://doi.org/10.5194/hess-18-1575-2014

Saxton, K. E., & Rawls, W. J. (2006). Soil water characteristic estimates by texture and organic matter for hydrologic solutions. *Soil Science Society of America Journal*, *70*(5), 1569–1578. https://doi.org/10.2136/sssaj2005.0117

Schneider, T., O'Gorman, P. A., & Levine, X. J. (2010). Water vapor and the dynamics of climate changes. *Reviews of Geophysics*, *48*(3), RG3001. https://doi.org/10.1029/2009RG000302

Seneviratne, S. I., Donat, M. G., Pitman, A. J., Knutti, R., & Wilby, R. L. (2016). Allowable CO_2 emissions based on regional and impact-related climate targets. *Nature*, *529*(7587), 477–483. https://doi.org/10.1038/nature16542

Seneviratne, S. I., Lüthi, D., Litschi, M., & Schär, C. (2006). Land–atmosphere coupling and climate change in Europe. *Nature*, *443*(7108), 205–209. https://doi.org/10.1038/nature05095

Sheffield, J., & Wood, E. F. (2008). Global trends and variability in soil moisture and drought characteristics, 1950–2000, from observation-driven simulations of the terrestrial hydrologic cycle. *Journal of Climate*, *21*(3), 432–458. https://doi.org/10.1175/2007JCLI1822.1

Sherwood, S., & Fu, Q. (2014). A drier future? *Science*, *343*(6172), 737–739. https://doi.org/10.1126/science.1247620

Smallman, T. L., & Williams, M. (2019). Description and validation of an intermediate complexity model for ecosystem photosynthesis and evapotranspiration: ACM-GPP-ETv1. *Geoscientific Model Development*, *12*(6), 2227–2253. https://doi.org/10.5194/gmd-12-2227-2019

Smettem, K. R. J. (1984). Soil-water residence time and solute uptake: 3. Mass transfer under simulated winter rainfall conditions in undisturbed soil cores. *Journal of Hydrology*, *67*(1–4), 235–248. https://doi.org/10.1016/0022-1694(84)90243-9

Song, J., Wan, S., Piao, S., Knapp, A. K., Classen, A. T., Vicca, S., et al. (2019). A meta-analysis of 1,119 manipulative experiments on terrestrial carbon-cycling responses to global change. *Nature Ecology & Evolution*, *3*(9), 1309–1320. https://doi.org/10.1038/s41559-019-0958-3

Sprenger, M., Stumpp, C., Weiler, M., Aeschbach, W., Allen, S. T., Benettin, P., et al. (2019). The demographics of water: A review of water ages in the critical zone. *Reviews of Geophysics*, *57*(3), 800–834. https://doi.org/10.1029/2018RG000633

Tang, Q., Oki, T., Kanae, S., & Hu, H. (2007). The influence of precipitation variability and partial irrigation within grid cells on a hydrological simulation. *Journal of Hydrometeorology*, *8*(3), 499–512. https://doi.org/10.1175/JHM589.1

Trenberth, K. E., Dai, A., Rasmussen, R. M., & Parsons, D. B. (2003). The changing character of precipitation. *Bulletin of the American Meteorological Society*, *84*(9), 1205–1218. https://doi.org/10.1175/BAMS-84-9-1205

Trenberth, K. E., & Zhang, Y. (2018). How often does it really rain? *Bulletin of the American Meteorological Society*, *99*(2), 289–298. https://doi.org/10.1175/BAMS-D-17-0107.1

Vereecken, H., Huisman, J. A., Bogena, H., Vanderborght, J., Vrugt, J. A., & Hopmans, J. W. (2008). On the value of soil moisture measurements in vadose zone hydrology: A review. *Water Resources Research*, *44*(4). https://doi.org/10.1029/2008WR006829

Walker, A. P., De Kauwe, M. G., Bastos, A., Belmecheri, S., Georgiou, K., Keeling, R. F., et al. (2021). Integrating the evidence for a terrestrial carbon sink caused by increasing atmospheric CO_2. *New Phytologist*, *229*(5), 2413–2445. https://doi.org/10.1111/nph.16866

Wang, J., Chen, X., Hu, Q., & Liu, J. (2020). Responses of terrestrial water storage to climate variation in the Tibetan Plateau. *Journal of Hydrology*, *584*, 124652. https://doi.org/10.1016/j.jhydrol.2020.124652

Wang, K., & Dickinson, R. E. (2012). A review of global terrestrial evapotranspiration: Observation, modeling, climatology, and climatic variability. *Reviews of Geophysics*, *50*(2). https://doi.org/10.1029/2011RG000373

Wu, P., Christidis, N., & Stott, P. (2013). Anthropogenic impact on Earth's hydrological cycle. *Nature Climate Change*, *3*(9), 807–810. https://doi.org/10.1038/nclimate1932

Yan, J., Bogie, N. A., & Ghezzehei, T. A. (2020). Root uptake under mismatched distributions of water and nutrients in the root zone. *Biogeosciences*, *17*(24), 6377–6392. https://doi.org/10.5194/bg-17-6377-2020

Yang, D., Yang, Y., & Xia, J. (2021). Hydrological cycle and water resources in a changing world: A review. *Geography and Sustainability*, *2*(2), 115–122. https://doi.org/10.1016/j.geosus.2021.05.003

Yang, Y., Guan, H., Batelaan, O., McVicar, T. R., Long, D., Piao, S., et al. (2016). Contrasting responses of water use efficiency to drought across global terrestrial ecosystems. *Scientific Reports*, *6*(1), 23284. https://doi.org/10.1038/srep23284

Yeh, J.-F., & Wu, C. (2018). Recent acceleration of the terrestrial hydrologic cycle in the U.S. Midwest. *Journal of Geophysical Research: Atmospheres*, *123*(6), 2993–3008. https://doi.org/10.1002/2017JD027706

Yin, D., Roderick, M. L., Leech, G., Sun, F., & Huang, Y. (2014). The contribution of reduction in evaporative cooling to higher surface air temperatures during drought: Drought and temperature. *Geophysical Research Letters*, *41*(22), 7891–7897. https://doi.org/10.1002/2014GL062039

Zhu, Z., Piao, S., Myneni, R. B., Huang, M., Zeng, Z., Canadell, J. G., et al. (2016). Greening of the Earth and its drivers. *Nature Climate Change*, *6*(8), 791–795. https://doi.org/10.1038/nclimate3004